

## Magnetostratigraphy and rock magnetism of the Ilerdian stratotype at Tremp, Spain

J.O. Pascual<sup>a</sup>, J.M. Parés<sup>a</sup>, C.G. Langereis<sup>b</sup> and J.D.A. Zijdeveld<sup>b</sup>

<sup>a</sup> Institute of Earth Sciences “Jaume Almera”, C.S.I.C. Martí i Franqués s/n, 08028 Barcelona, Spain

<sup>b</sup> Paleomagnetic Laboratory, Fort Hoofddijk, Budapestlaan 17, 3584 CD Utrecht, Netherlands

(Received 19 February 1992; revision accepted 29 June 1992)

### ABSTRACT

Pascual, J.O., Parés, J.M., Langereis, C.G. and Zijdeveld, J.D.A., 1992. Magnetostratigraphy and rock magnetism of the Ilerdian stratotype at Tremp, Spain. *Phys. Earth Planet. Inter.*, 74: 139–157.

The first magnetic polarity stratigraphy of the Ilerdian stratotype locality—the Tremp section, Spain—has been established. In total, 315 samples from 66 levels have been demagnetized, both thermally and by alternating field. Various types of (rock) magnetic behaviors and (low- and high-temperature) magnetization components have been distinguished, and have been correlated with the three sampled rock types: clays, marls and fine-grained sandstones, and coarse-grained sandstones. The paleomagnetic directions have been classified according to their reliability in representing a primary magnetization. The magnetostratigraphy of the Tremp section is characterized by a long reversed polarity zone interrupted by a normal zone. We conclude that the normal polarity interval found in the Ilerdian stratotype may represent Chron 24.2. The lower and upper reversed intervals of the section are then respectively Chrons 24.1R and 24R.

### 1. Introduction

The first proposition of the Ilerdian as a new Stage of the (earliest) Eocene was made by Hottinger and Schaub (1960), based on the fact that in the Paris basin there are no *Nummulites*, *Alveolina* or other larger foraminifera below the Cuisian (early Eocene), whereas in other areas—the Pyrenees, Swiss Alps, Asia Minor and North Africa—larger foraminifera were found as phylogenetic precursors to those of the Cuisian, but were more evolved than those of the Thanetian (late Paleocene). The Ilerdian Stage was biochronostratigraphically defined by Schaub (1969) based on the larger foraminifera. The stratotype section is the Tremp section, characterized by its accessibility and quality of exposure along

the road section between Tremp and Pont de Montanyana, from the village of Claret almost to the Montllobar mountain pass (Conca de Tremp, Pyrenees, Spain) (Fig. 1). The Ilerdian deposits of the Tremp section are interpreted as a transgressive–regressive shallow marine coarsening upwards succession, its sedimentation being strongly influenced by the Sant Corneli–Boixols thrust located to the north.

For the biozonation of the Ilerdian by larger foraminifera, Schaub (1981) synthesized the previous work and divided the stage in three intervals each of which is defined by specific biozones:

Upper Ilerdian:

*Alveolina trempina*, *Nummulites involutus* and *Assilina adrianensis*

Middle Ilerdian:

*Alveolina corbarica*, *Nummulites exilis* and *Assilina leymeriei*;

*Alveolina moussoulensis*, *Nummulites robustiformis* and *Assilina* aff. *arenensis*

Correspondence to: J.O. Pascual, Institute of Earth Sciences “Jaume Almera”, C.S.I.C. Martí i Franqués s/n, 08028 Barcelona, Spain.

#### Lower Ilerdian:

*Alveolina ellipsoidalis*, *Nummulites fraasi* and *Assilina arenensis*;

*Alveolina cucumiformis*, *Nummulites fraasi* and *Assilina prisca*

Recently, Pascual et al. (1991) have determined, in the Tremp section, all the species related to the genera *Alveolina*, *Assilina* and *Nummulites*, to differentiate the biozones (Fig. 2). Although not all biozones described by Hottinger and Schaub (1960) were recognized in this stratotype, it is possible to correlate the lithostratigraphy of the section with carbonate shelves which are developed to the south of the Tremp section (richer in *Alveolina* genus), and then deduce the existence and correlation of all the biozones.

The Ilerdian stratotype has not been accepted as an International Standard Stage (ISS), mainly because the section is set between continental facies, and also because it is poor in planktonic foraminifera and in calcareous nannofossils,

which are the main groups used in the general correlation scales. Therefore, it is not possible to define the upper and lower marine boundaries and hence it is very difficult to place the section in the geological time-scale. This problem was solved by Schaub (1969), who designated the Campo section (Huesca province) as the parastratotype.

Recent chronostratigraphic scales (Berggren et al., 1985; Aubry et al., 1988) consider only the Ypresian Stage for the early Eocene. Steurbaut (1988) placed the Ypresian in the calcareous nannofossil zones NP11, NP12, NP13 and the lower part of NP14, with the Cuisian completely overlapping the early Ypresian. Cavelier and Pomerol (1986) also overlapped the Cuisian with the early Ypresian (*sensu lato*) but the bottom of these two stages does not adjust to the base of the lower Eocene. The latter workers placed the bottom of the Ilerdian at the Paleocene–Eocene boundary and overlapped the middle and upper part of the

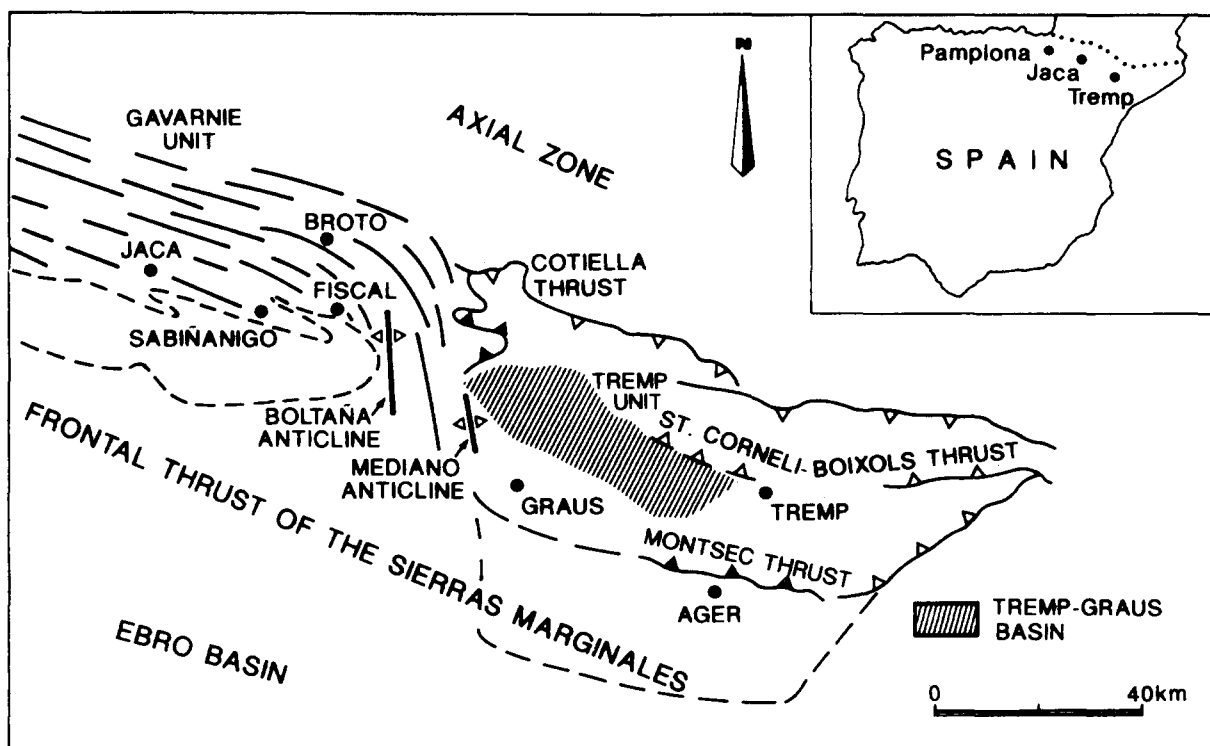


Fig. 1. Geological scheme of the Jaca–Tremp area, which includes the Tremp–Graus Basin (modified after Mutti et al. (1988)). In the western area, lines represent major structural trends and dashed lines limit the allochthonous Paleogene.

Illeridian with the lower Ypresian. According to the calcareous nannofossils studied by Wilcoxon (1973) and Kapellos and Schaub (1973, 1975), the various assemblages recognized in the Illeridian are zones NP9, NP10, NP11 and NP12 of Martini (1971), although the existence of the NP12 biozone at the top of the Illeridian stratotype is questionable (Molina et al., 1992).

The Thanetian and Selandian are two standard stages located in the Paleocene, but neither of them overlaps with the upper part of the late Paleocene. The top of the Thanetian is located in NP8–NP9 (Curry, 1981; Hamilton and Hojatzadeh, 1982), and data for the Selandian (Perch-Nielsen and Hasen, 1981) reveal that the top could correspond to the lower part of NP9.

Consequently, the Illeridian is located at the Paleocene–Eocene boundary and covers the gap between the Thanetian and the Ypresian. Considering the above-mentioned calcareous nannofossil biozones, the upper Illeridian could cross into the Ypresian. There is no general agreement on the exact position of the Paleocene–Eocene boundary in the geologic time-scale, and it must therefore be restudied. Meanwhile, the Paleocene–Eocene boundary used today has different locations depending on the focus of interest of the researchers.

The stratotype of the Illeridian in the Tremp Basin was chosen for the present study because no magnetostratigraphy of the corresponding stratotypes has yet been established, although there have been several attempts to correlate Tertiary sections along the southern Pyrenees. The intention of this study is to correlate the Illeridian Stage with the geomagnetic polarity time-scale (GPTS) and to establish the position of the foraminiferal zones.

## 2. Geological setting, biostratigraphy and sampling

The Pyrenean Belt extends from Provence (France) in the east to the Cantabrian Platform (NW Spain) in the west. It is Alpine in age although its structures do not show continuity with those of the Alpine Mediterranean orogenic

belt. A thrust and fold system developed during the Alpine compression. The western Pyrenees are characterized by north-directed thrusts, whereas in the central and eastern Pyrenees the thrusts are arranged in a system of antiformal thrusts in the so-called axial zone, bounded to the south by south-directed imbricated thrust systems. The southern thrust sheets in the central Pyrenees consist of cover rocks of Mesozoic and Tertiary age with the system propagation being piggyback in style (Fig. 1). Tertiary examples include Cotiella, St. Corneli–Boixols, Montsec and Sierras Marginales. In the southern Pyrenees, a foreland basin—the Ebro Basin—developed ahead of the moving thrust sheets from the earliest stages of deformation. As the deformation progressed southwards, the foreland basin also migrated in this direction to become progressively incorporated into the younger thrust sheets, giving rise to the South Pyrenean basin (Souquet et al., 1977; Williams, 1985; Puigdefàbregas and Souquet, 1986). The eastern part of this basin is called the Tremp–Graus Basin, where the Illeridian was defined.

The Illeridian stratotype has been well studied biostratigraphically (Hottinger, 1960; Hottinger et al., 1964; Caro, 1973; Luterbacher, 1973; Wilcoxon, 1973; Kapellos and Schaub, 1973, 1975; Ferrer et al., 1973; Von Hillebrandt, 1975), stratigraphically (Mey et al., 1968; Mutti et al., 1972; Gaemers, 1978; Fonnesu, 1984) and sedimentologically (Fonnesu, 1984). In our study, the stratigraphic section was measured and described concurrently with the paleomagnetic sampling. The length of the section was measured perpendicular to the strike using a Jacob's staff. Paleomagnetic sites were spaced at intervals of 7–9 m and at least six specimens were taken at each site. The weathered surface was carefully removed to drill fresh samples, and sampling was carried out with a portable electrically powered drill. The samples were oriented using a Silva compass with clinometer.

## 3. Rock magnetism

A number of rock magnetic properties have been determined to qualify and identify the mag-

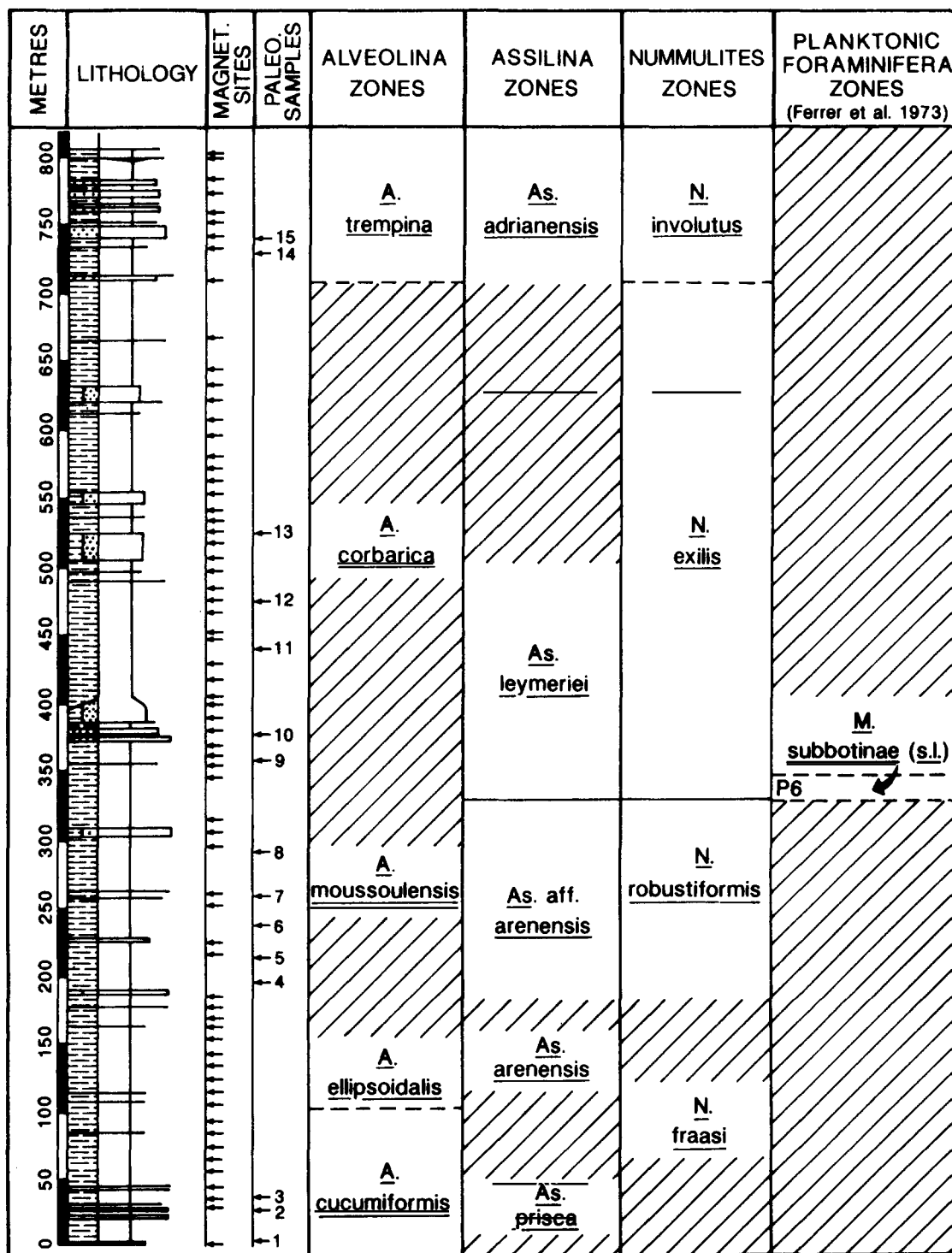


Fig. 2. Lithology and biozones of the Tresp section recognized by Hottinger and Schaub (1960) in the Ilirian stratotype. The hatched shading represents those biozones which have not been found by Pascual et al. (1991).

netomineralogy and/or magnetic characteristics that correspond to the various types of rocks: (1) marls and fine-grained sandstones; (2) clays; (3) coarse-grained sandstones. These rock magnetic experiments include isothermal remanent magnetization (IRM) acquisition—both uniaxially and in three orthogonal directions—and subsequent thermal demagnetization, monitoring of initial susceptibility ( $X_{in}$ ) during thermal demagnetization, and anhysteretic remanent magnetization (ARM) behaviour.

### *3.1. IRM acquisition and susceptibility changes during thermal demagnetization of IRM*

#### *3.1.1. Marls and fine-grained sandstones*

The acquisition of IRM in fields up to 2000 mT of essentially all marls and fine-grained sandstones (Fig. 3(a)) shows an initial steep rise until approximately 200 mT (acquiring more than 80% of the maximum IRM), and saturation of the remaining 15–20% is reached in fields of 500 mT. The IRM thermal demagnetization curves (Fig. 3(b)) are characterized by a three-fold decay: a first rapid decrease between 100 and 150°C, another between 300 and 330°C, and finally a more gradual decrease with a maximum unblocking temperature at 570–580°C. This indicates the presence of three magnetic phases with blocking temperature spectra that have maximum unblocking temperatures of approximately 150, 320 and 580°C. In the susceptibility curves,  $X_{in}$  strongly increases between 360 and 400°C, and reaches a maximum at 480–500°C before finally decreasing again. At the highest temperatures (700°C), values still much higher than at room temperature are found.

In the IRM thermal decay curves (Fig. 3(b)), the first decrease may indicate an irreversible alteration rather than maximum blocking temperatures of a separate magnetic phase. A similar alteration at 150°C was found by Van Velzen and Zijdeveld (1992) in early Pliocene marls. These researchers suggested that the alteration, which was accompanied by a decay of IRM and a reduction of coercivities higher than 100 mT, was due to the reduction of stresses in superficially maghemitized magnetite grains. Weathering of

the rocks could explain such a slight maghemitization. There is no noticeable change in  $X_{in}$  during this first decrease.

The second decay, at 300–360°C, possibly corresponds to an iron sulfide (pyrrhotite or greigite; see Dekkers, 1990), but it may also indicate the presence of maghemite. The existence of maghemite is possible as a result of low-temperature oxidation of magnetite to maghemite (Heider and Dunlop, 1987; Özdemir, 1990) caused by weathering in the field. No firm discrimination can be made on the basis of the IRM acquisition results (Fig. 3(a)), as the rapid increase between 0 and 200 mT could indicate both magnetite and maghemite. The existence of authigenic pyrrhotite is more common in magmatic rocks than in sediments. A primary magnetization caused by (authigenic) pyrrhotite has been reported in sediments (Linssen, 1988; Kligfield and Channell, 1981), although it is usually found that stable authigenic iron sulfides are restricted to pyrite, mackinawite and greigite (Morse et al., 1987). Authigenic pyrrhotite in sedimentary basins can form only in relation to hydrothermal fluids (Deer et al., 1966) and in reducing basins (Hsieh and West, 1981; Casagrande, 1987). The presence of detrital pyrrhotite in the study area is unlikely because the area is not close to any magmatic or metamorphic source and because of the instability of detrital pyrrhotite in the Eh/pH equilibrium conditions which prevail in the studied basin (Brookins, 1988). The characteristics of the acquisition curve between 200 and 500 mT could indicate the existence of a magnetic iron sulfide (Dekkers, 1990). If the second decrease in the IRM thermal decay curve (at 320°C) corresponds to an iron sulfide, the strong increase in susceptibility at 360–400°C (Fig. 3(c)) could be explained by the sulfide becoming unstable during thermal demagnetization and being oxidized to magnetite, or by the typical oxidation of pyrite to magnetite. The large increase in susceptibility is possible only if a considerable amount of single domain (SD) magnetite is produced and/or if the new magnetite is very fine grained and is thus superparamagnetic (SP). Only part of the newly formed magnetite is oxidized to hematite upon further heating, considering the still higher than initial  $X_{in}$  values at

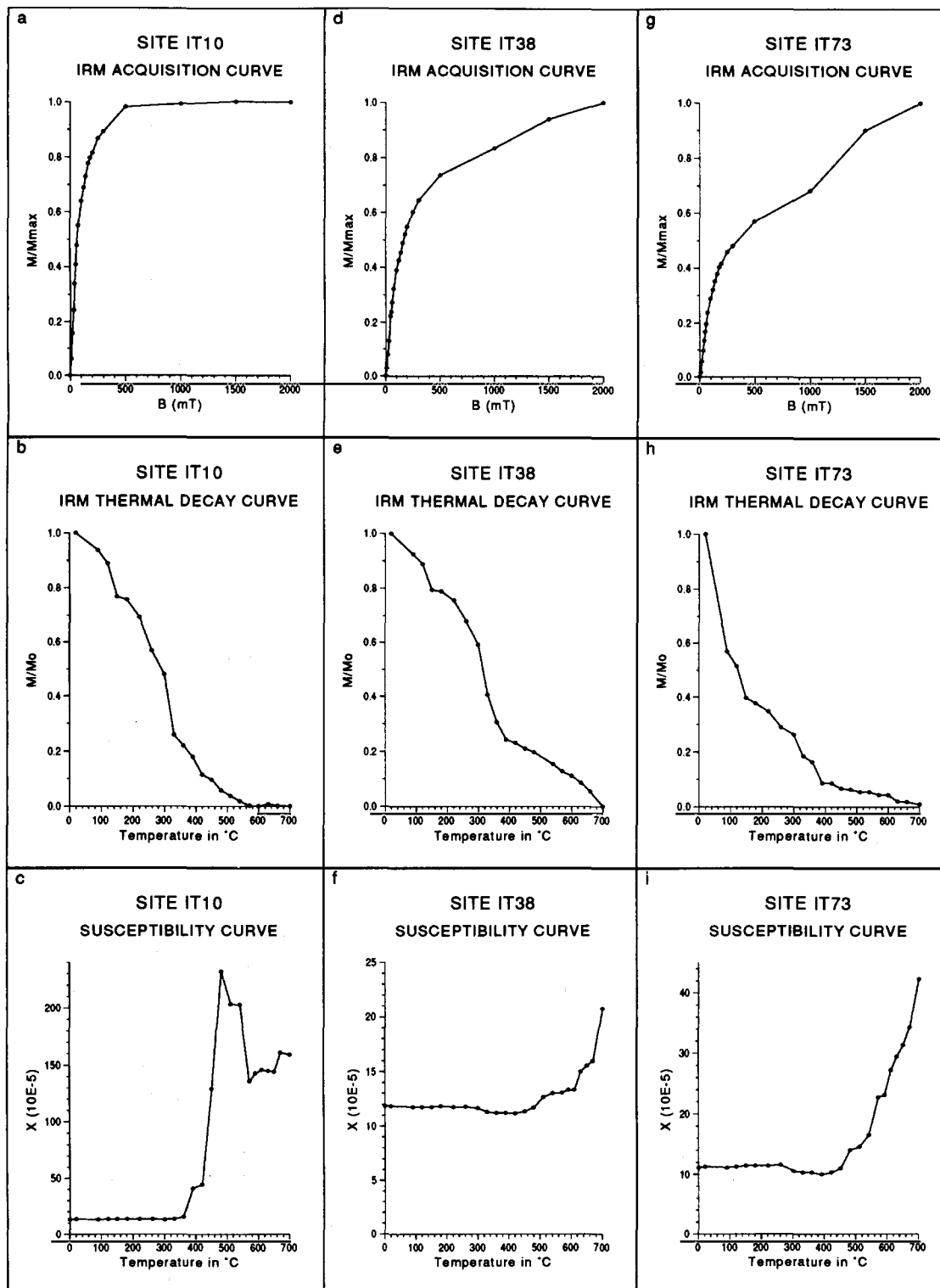


Fig. 3. Acquisition and thermal demagnetization of IRM and corresponding susceptibility changes. The association (a)–(b)–(c) is typical for marls and fine-grained sandstones, (d)–(e)–(f) for clays, and (g)–(h)–(i) for coarse-grained sandstones.

the highest temperatures. The highest unblocking temperatures (570–580°C) typically represent magnetite, but only some 20% of the total IRM is carried by this mineral.

### 3.1.2. Clays

The acquisition of the IRM in clays (Fig. 3(d)) shows an initial steep rise until 200 mT, and a

less steep rise until 500 mT, after which the IRM gradually increases, but saturation is not reached in the highest field (2000 mT). In the IRM thermal decay curves (Fig. 3(e)), the first decay occurs at 150°C, the second at 330–360°C, the third—which is not always clearly noticeable—between 570 and 600°C, and the highest unblocking temperatures are found between 660 and 700°C. In

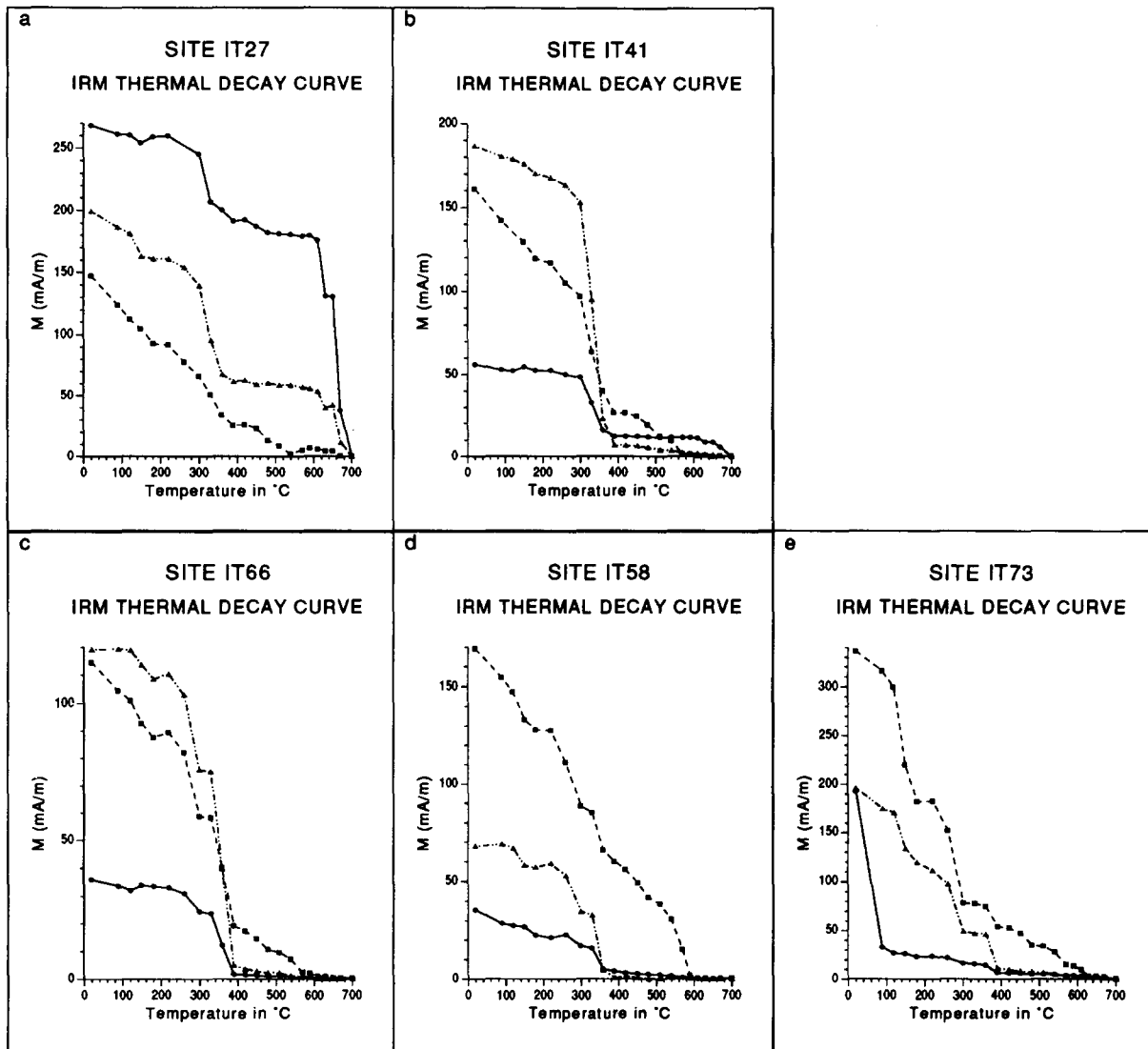


Fig. 4. Thermal demagnetization of IRM acquired in three orthogonal directions with different field strengths (Lowrie, 1990). Squares and dashed lines represent coercivities between 0 and 120 mT; triangles and dotted lines coercivities between 120 and 500 mT; circles and solid lines coercivities between 500 and 1500 mT. Clays typically show behavior as in (a) and (b), marls and fine-grained sandstones as in (c) and sometimes as in (d), and coarse-grained sandstones as in (e).

the susceptibility curves (Fig. 3(f)), a small decrease ( $\pm 10\%$ ) after  $300^\circ\text{C}$  is seen, then  $X_{\text{in}}$  starts to increase slowly between  $420$  and  $480^\circ\text{C}$ , followed by a smooth peak at  $520$ – $580^\circ\text{C}$  before  $X_{\text{in}}$  increases again at higher temperatures.

The interpretation of the first, second and third phases in the IRM thermal decay curve is the same as for those of the marls and fine-grained sandstones, although the contribution of magnetite seems somewhat smaller ( $\pm 10\%$ ). The small decrease in susceptibility after  $330^\circ\text{C}$  (Fig. 3(f)) has been related to the existence of sulfides (Dekkers, 1990; Krs et al., 1992). The maximum unblocking temperatures of  $660$ – $700^\circ\text{C}$  (Fig. 3(e)) and lack of saturation of the IRM (Fig. 3(d)) point to the presence of hematite.

### 3.1.3. Coarse-grained sandstones

The behavior of the coarse-grained sandstones is completely different from that of the other two rock types. The IRM acquisition curves (Fig. 3(g)) rise steeply at first until  $200$  mT, then increase slowly with a slight inflection at  $1000$  mT, but saturation is not reached. Thermal demagnetization of the IRM (Fig. 3(h)) shows the presence of goethite: it can be seen that  $50\%$  of the rema-

nence is rapidly removed at  $100^\circ\text{C}$ , in accordance with the very low Néel temperatures of goethite ( $60$ – $120^\circ\text{C}$ ). The second phase is located at  $150^\circ\text{C}$ , i.e. the same temperature as for the marls, clays and fine-grained sandstones. The third phase, with unblocking temperatures of  $360$ – $390^\circ\text{C}$ , is observed to occur in the temperature range of the goethite dehydration reaction (Dekkers, 1988). The curve then decreases slowly until  $630^\circ\text{C}$ , where an additional decay can be seen which may be typical for cation-deficient magnetic or maghemite (Heider and Dunlop, 1987). Finally, the highest unblocking temperatures are found at  $680$ – $700^\circ\text{C}$ ; this indicates the presence of (a small amount of) hematite. The susceptibility curves (Fig. 3(i)) show a very small decrease after  $260^\circ\text{C}$ . At higher temperatures ( $420$ – $450^\circ\text{C}$ ), the susceptibility increases considerably, as a result of the creation of trace amounts of magnetite (Dekkers, 1988).

### 3.2. IRM acquisition and thermal demagnetization in three orthogonal directions

Following the method of Lowrie (1990), we have applied an IRM in three orthogonal direc-

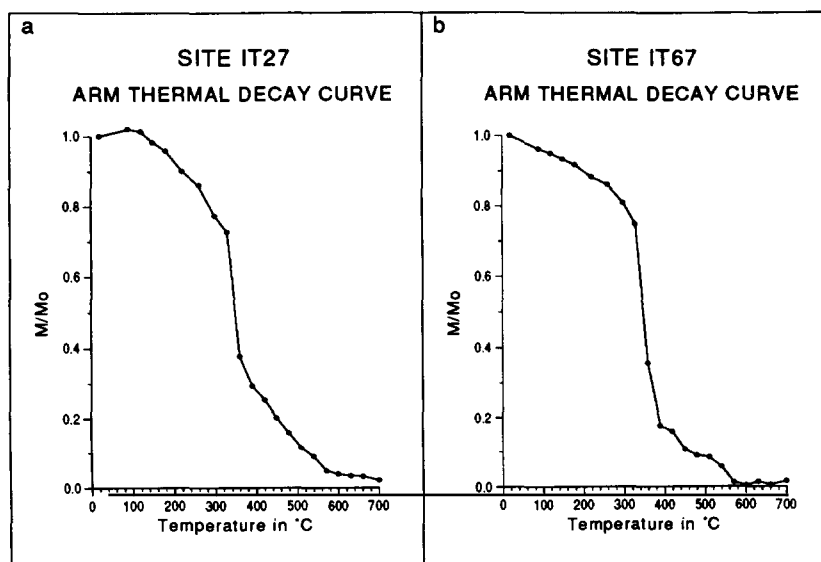


Fig. 5. Thermal decay curves of ARM, introduced by using an a.f. of  $300$  mT on which a direct field of  $38 \mu\text{T}$  was superimposed. There is no relation between the various ARM behaviors and the rock types.



tions, to study the coercivity fractions, in samples of all three rock types. The applied fields are 120 mT (low-coercivity (LC) fraction), 500 mT

(medium-coercivity (MC) fraction) and 1500 mT (high-coercivity (HC) fraction); the IRM thus obtained was subsequently thermally demagnetized

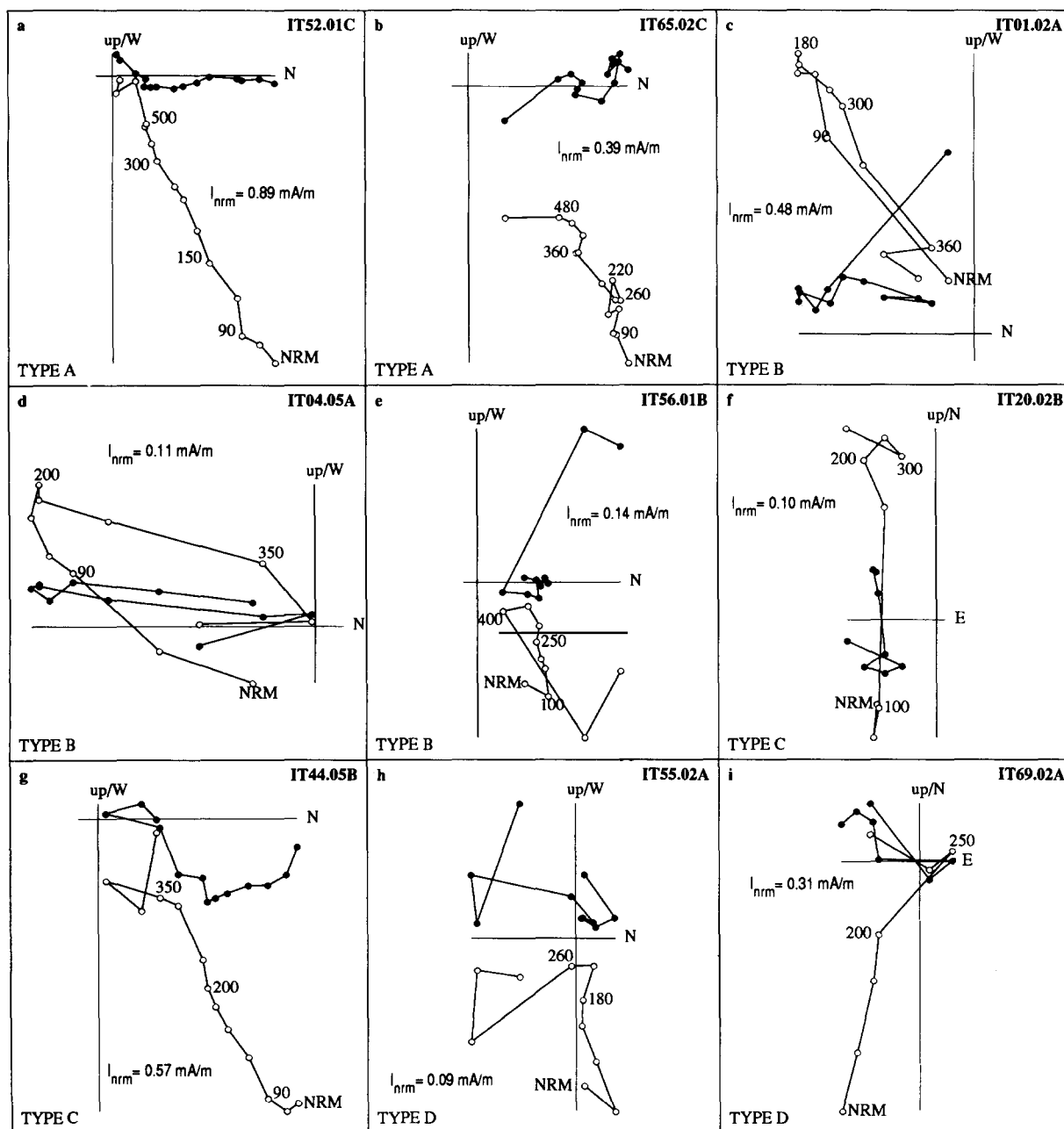


Fig. 6. Thermal demagnetization vector diagrams. Solid circles represent projection on the horizontal plane, and open circles projection on the vertical plane. Numbers denote the temperature steps.

(Fig. 4). There is a relation between the behavior of the curves and the rock types, but it is not as clear as that found above.

### 3.2.1. Clays

Clays behave as shown in Figs. 4(a) and 4(b). Figure 4(a) shows a sharp decrease at 330–360°C mainly in the MC and HC fractions, whereas in Fig. 4(b) all coercivity fractions show a sharp

decrease at these temperatures, indicating the existence of a mineral that is represented in each fraction. Thermally, this mineral could be sulfide or maghemite, but the presence of pyrrhotite or greigite in the HC fraction is difficult to explain. Nevertheless, Lowrie (1990, Fig. 4) interpreted such behavior as typical for pyrrhotite. The presence of magnetite is clear from the curves that represent the LC and (partly) the MC fraction.

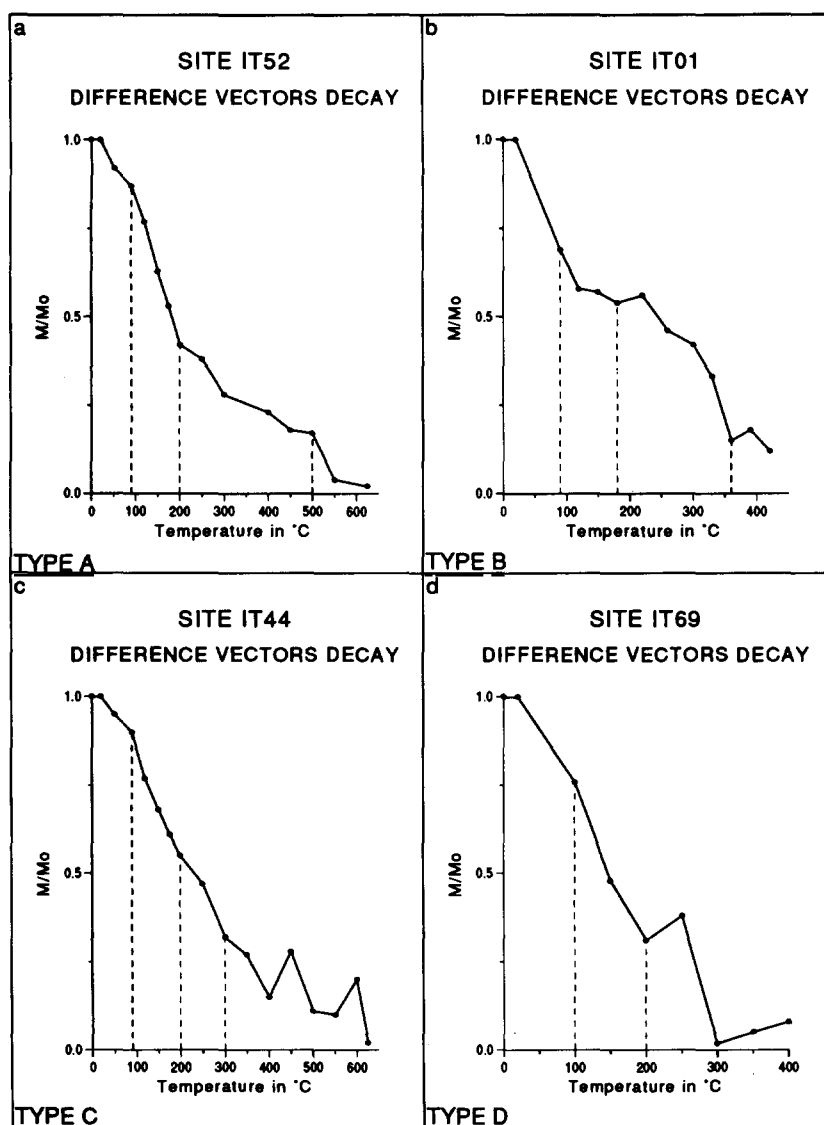


Fig. 7. Thermal decay curves using the sum of difference vectors between successive demagnetization steps. Vertical dashed lines represent the approximate boundaries of the temperature spectra of the various components discussed in the text.

The HC decay curves show clearly the presence of hematite; in Fig. 4(a) the contribution of hematite is considerable.

### 3.2.2. *Marls and fine-grained sandstones*

They behave as shown in Fig. 4(c), and sometimes as in Fig. 4(d). The interpretation of Fig. 4(c) is the same as that of Fig. 4(b), but in this case there is no evidence for hematite. The presence of magnetite is clearly indicated, either in the MC fraction (Fig. 4(c)) or in the LC fraction (Fig. 4(d)). This implies a slightly different magnetite coercivity range in the various samples, most probably related to a (slightly) different grain-size. The results agree well with the conclusions obtained from the acquisition and demagnetization of IRM and susceptibility during thermal demagnetization.

### 3.2.3. *Coarse-grained sandstones*

These behave only as shown in Fig. 4(e). The presence of goethite is clearly indicated in the HC fraction decay curve by a very strong decrease at 90°C. The LC and MC fractions show unblocking temperatures between 300 and 390°C, which may indicate the temperature range of the goethite dehydration reaction (Dekkers, 1988). The presence of cation-deficient magnetite or maghemite is strongly suggested by the unblocking temperatures of 630°C, similar to those mentioned in Section 3.1. Only a trace amount of hematite is indicated by the highest unblocking temperatures of 680°C.

## 3.3. *ARM behavior*

An ARM was introduced by using an alternating field (a.f.) of 300 mT, on which a direct field of 38  $\mu$ T was superimposed. The ARM was subsequently thermally demagnetized. There appears to be no clear relation between the various ARM thermal decay curves and the rock types. Two classes of magnetic behavior have been recognized (Figs. 5(a) and 5(b)). Both show a major decrease in intensity at 360–390°C, indicating an iron sulfide and/or maghemite. A second decay at 570–580°C corresponds to magnetite. Only in some samples (Fig. 5(a)), do higher unblocking

temperatures (680–700°C) indicate the presence of hematite.

## 4. *NRM components and magnetostratigraphy*

To establish the magnetostratigraphy of the selected section, we have demagnetized 315 specimens from 66 sites. Thermal demagnetization using small temperature increments (50, 40 and 30°C) was applied to 283 specimens, and 32 specimens were treated by a.f. demagnetization. The natural remanent magnetization (NRM) was measured using both a CCL (UK) cryogenic magnetometer (at Barcelona) and a 2G (USA) cryogenic magnetometer (at Utrecht). The directions of the characteristic remanent magnetization (ChRM) were analyzed by least-squares fit of a line (Kirschvink, 1980) through selected data points.

### 4.1. *NRM components*

All treated samples show a viscous component that is removed at 90–100°C (Figs. 6 and 7); it is probably induced by drilling and/or is the result of storage in the laboratory. A further component is removed at 180–220°C; its direction is the same as the present-day magnetic field (Fig. 6); it is most likely of secondary origin, caused by weathering. For the higher-temperature (HT) or characteristic component(s), four types of magnetic behavior have been recognized.

Type A samples (Figs. 6(a), 6(b) and 7(a)) show an HT component which is removed between 180–220 and 550–600°C. The direction of this component coincides with that of the present-day magnetic field. Type B samples (Figs. 6(c)–6(e) and 7(b)) show a characteristic low-temperature (LT) component removed between 180–220 and 350–380°C. At higher temperatures there is either a cluster or the magnetization becomes randomly orientated and often strongly viscous. Type C samples (Figs. 6(f), 6(g) and 7(c)) also show a ChRM component in the same temperature range as type B, but only in the first stages. Above approximately 300°C the magnetization becomes random or shows a medium-temperature (MT) cluster. Finally, type D samples (Figs. 6(h), 6(i)

and 7(d)) are characterized as having only a secondary component and then a LT cluster or a random magnetization. In general, sandstones show type A and D behavior, whereas clays,

marls and fine-grained sandstones show type B and C behavior.

The clusters have been studied in further detail (Fig. 8). The mean direction obtained from

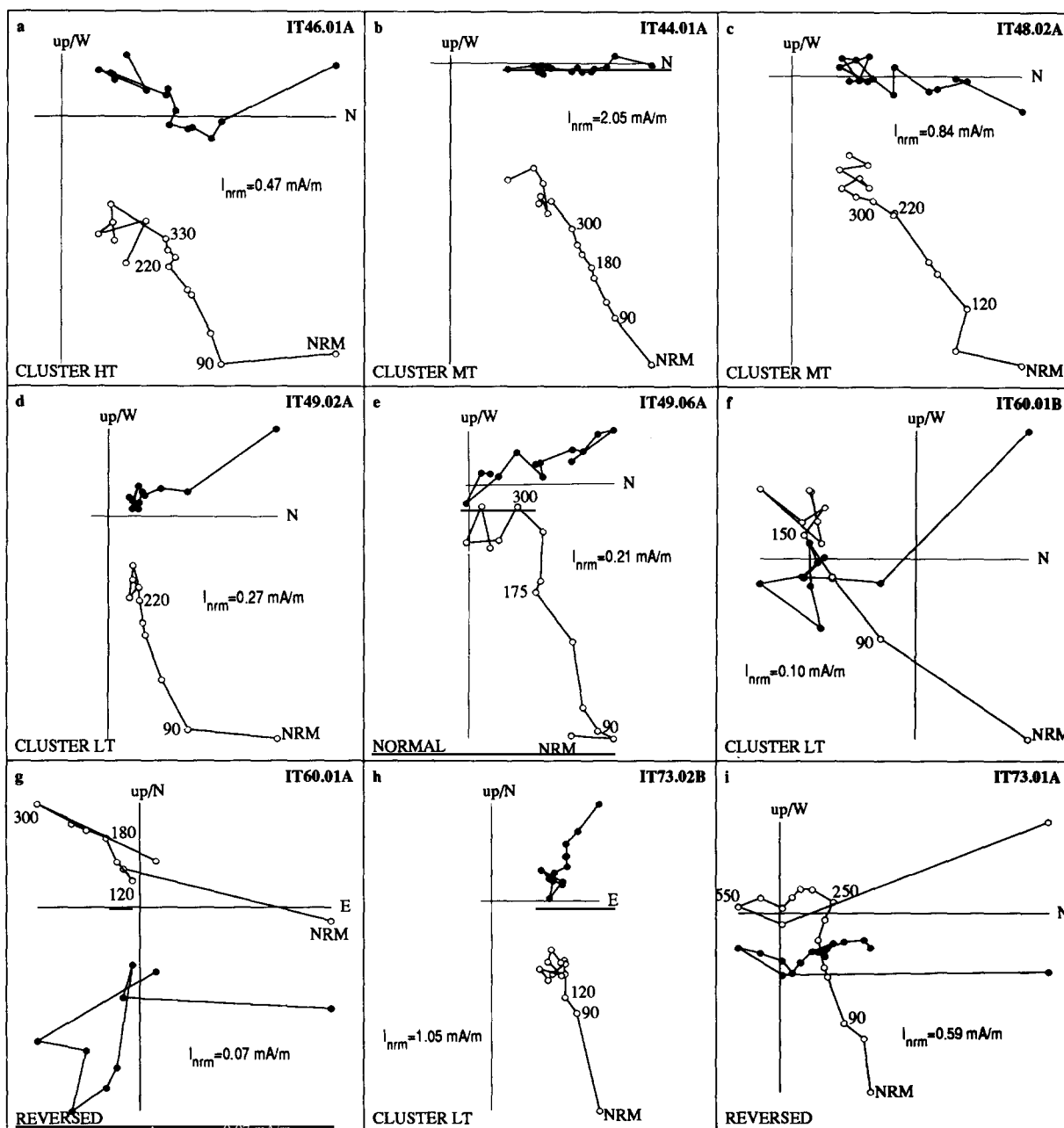


Fig. 8. Thermal demagnetization diagrams, showing cluster behavior at high (a), medium (b) and (c), as well as at low (d), (f) and (h) temperatures. Symbols and numbers are as in Fig. 7.

the HT clusters (Fig. 8(a)) and MT clusters (Figs. 8(b) and 8(c)) agree with the polarity obtained in samples from the same site which do not show a cluster. In Figs. 8(d) and 8(e) there is an example from site IT49, where specimen 02A has a north-directed LT cluster, whereas specimen 06A has no cluster and a characteristic north-directed component, decaying towards the origin. An example from site IT60 (Figs. 8(f) and 8(g)) shows a south-directed LT cluster in specimen 01B, and the same direction is found in the characteristic

component of specimen 01A. The direction and polarity obtained from LT clusters do not agree with the direction and polarity for samples from the same site. Sample IT73 (Figs. 8(h) and 8(i)) is a case in which we have a north-directed LT cluster in specimen 02B, whereas specimen 01A has a south-directed characteristic component. As a result of this phenomenon, clusters have not been used for magnetostratigraphic purposes, or to calculate the mean direction.

The a.f. demagnetization shows three compo-

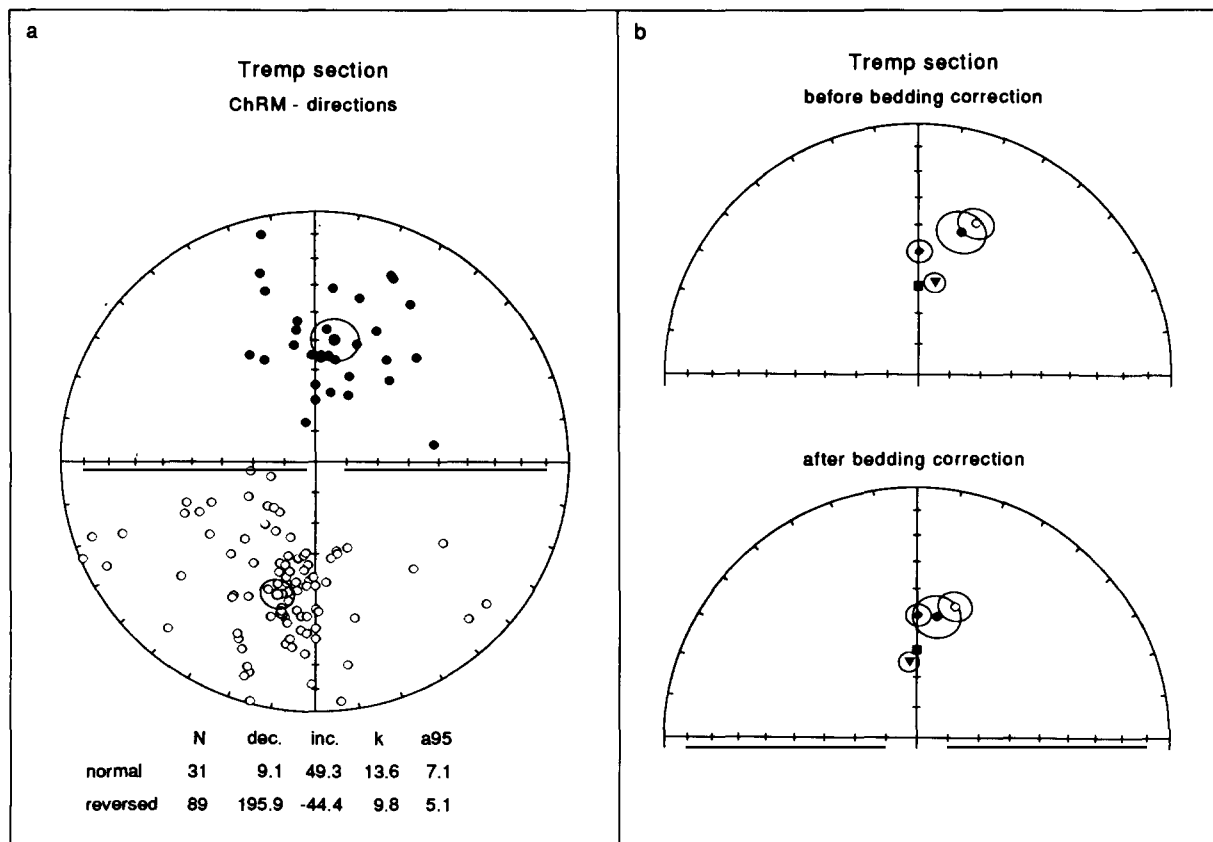


Fig. 9. (a) Equal-area projection of 'reliable' ChRM directions and their means after bedding tilt correction; open (closed) circles correspond to reversed (normal) polarities. (b) Mean inverted reversed (open circle) and mean normal (closed circle) directions of the Tremp section, mean direction of the secondary component (triangle), Eocene reference direction (Van der Voo, 1990; diamond) and geocentric axial dipole field direction for the present latitude of the study area (square), both before and after bedding tilt correction. Before bedding tilt correction, the Tremp directions are close to the Eocene direction and the secondary component is close to the axial dipole field. After bedding tilt correction, there is better agreement of the Tremp directions with the Eocene direction, supporting the idea that the mean direction obtained in Tremp is Eocene in age.

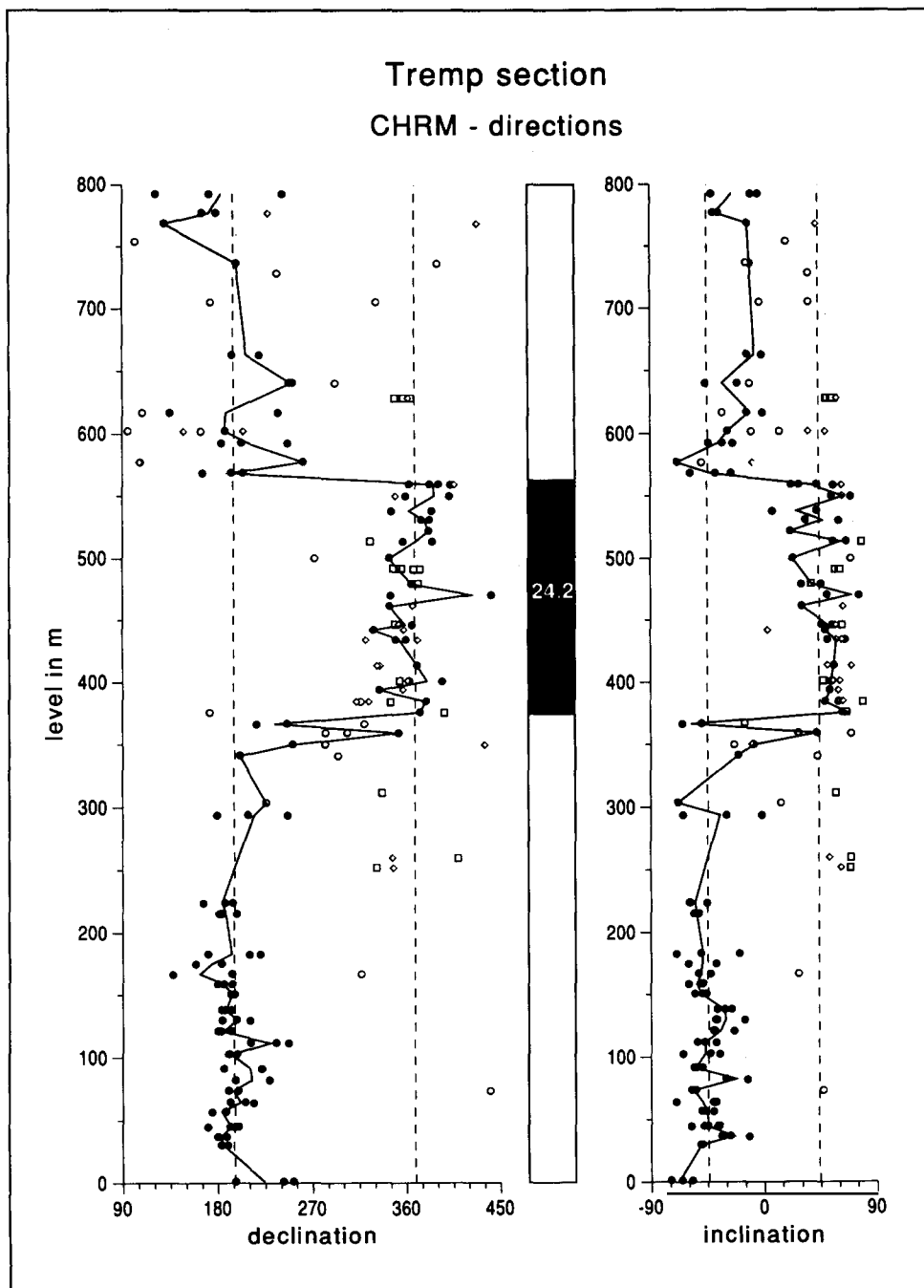


Fig. 10. ChRM directions and resulting magnetostratigraphy of the Ilerdian stratotype section. Solid and open circles denote 'reliable' and 'unreliable' directions, respectively, diamonds denote cluster directions, and squares represent specimens in which the high-temperature (or high-coercivity) component is a secondary magnetization. The polarity interpretation (solid line) is based on 'reliable' directions.

nents of differing stability: a viscous component is removed at 1.5–2.0 mT; a secondary component is removed at 10–15 mT; a high-coercivity component is removed at 30–40 mT. Results obtained from a.f. demagnetization have not been used for magnetostratigraphy and mean direction analysis because both the low- and high-coercivity components carry the present-day magnetic field direction.

Four reliability classes of directions have been denoted on the basis of results from the best demagnetization diagrams for the lower part of the section. The majority of samples show a multicomponent remanence upon demagnetization (class 1). A viscous component is removed at 90–100°C, followed by a secondary component which is removed at 180–220°C. The characteristic component (ChRM) is removed up to a maximum temperature of 350–450°C. We consider this ChRM reliable if it shows (more or less) a regular and linear decay towards the origin, and if normal polarity directions show a blocking temperature spectrum similar to the spectrum of reversed samples. Some samples depart from the general ‘reliable’ behavior described above, and we have classified these samples as: (class 2) ‘unreliable’ samples, which give aberrant directions; (class 3) totally remagnetized samples; (class 4) samples that show a ‘cluster’. Reliable directions were used to calculate the mean direction and to establish the magnetostratigraphy; samples that gave unreliable directions, clusters and remagnetized samples were rejected both for magnetostratigraphy and mean direction analysis. Each reliability class has been given a different symbol in the magnetostratigraphy plot (see Fig. 10).

#### 4.2. ChRM directions and magnetostratigraphy

To calculate the mean direction of the Tremp section, only reliable ChRM directions have been used (Fig. 9(a)). Normal and reversed mean directions after tilt correction are as follows:

	<i>N</i>	<i>D</i>	<i>I</i>	<i>k</i>	<i>a</i> <sub>95</sub>
Normal	31	9.1	49.3	13.6	7.1
Reversed	89	195.9	–44.4	9.8	5.1

where *N* is the number of specimens, *D* and *I* are declination and inclination, respectively, and *k* and *a*<sub>95</sub> are Fisher’s precision parameter and the semi-angle of the cone of confidence at the 95% level, respectively. The mean directions of both polarities are antiparallel, although the number of reliable normal data is considerably smaller. In Fig. 9(b) we have plotted the ChRM directions, the mean direction of the secondary component, the Eocene reference direction and the present-day magnetic field in the study area, both before and after bedding tilt correction. The Eocene reference direction (*D* = 0.6, *I* = 49.3) has been obtained from the mean paleopoles for Europe (Van der Voo, 1990). Reversed ChRM directions have been inverted, for better comparison of normal and reversed mean directions. Before bedding tilt correction, the ChRM directions of the Tremp section are close to the Eocene direction, whereas the mean direction of the secondary component is close to that of the present-day magnetic field. After bedding correction, the agreement of the mean ChRM directions with the Eocene direction has improved. These results suggest that the mean ChRM direction obtained at Tremp is Eocene in age, although slightly clockwise rotated, and that the secondary component corresponds to the present-day magnetic field direction. The magnetostratigraphic record of the section is characterized by a long reversed polarity zone interrupted by a normal zone (Fig. 10). At level 359 m, the topmost part of the lower reversed zone, samples from one site seem to be of normal polarity.

#### 5. Discussion and conclusions

Reliable reversed directions dominate in the lower part of the section (Fig. 10), whereas towards the top of the section more unreliable directions occur. This change in quality of the data may be attributed to weathering processes: the section is a coarsening upwards succession, and thus the upper part is more susceptible to weathering and the subsequent alteration of minerals. A comparison of the mean directions from





the Tremp section with earlier results from the same area shows the following results:

	<i>D</i>	<i>I</i>	Reference
Tremp, N	9.1	49.3	This study
Tremp, R	195.9	−44.4	This study
Ripoll syncline	157.0	−52.5	Burbank and Puigdefàbregas (1985)
Ebro Basin, N	10.0	45.0	Pascual and Parés (1990)
Ebro Basin, R	206.0	−51.0	Pascual and Parés (1990)
Ebro Basin	22.7	51.8	Parés (1988); Parés et al. (1988)

The Tremp inclination values agree fairly well with previous results from Eocene rocks located in the Ripoll syncline in the Eastern Pyrenees, and with values obtained along the SE margin of the Ebro Basin. The reversal test of McFadden and McElhinny (1990) has been used to check the antipodality of the Tremp mean ChRM directions. Basically, this test provides an estimate of the critical angle  $\gamma_c$  between the mean directions of the two sample distributions ( $N_1$  and  $N_2$ ) at which the hypothesis of a common mean direction is rejected. The test is positive if the angle between the two means ( $\gamma$ ) does not exceed the critical angle ( $\gamma_c$ ); the latter depends on  $N_1$ ,  $N_2$  and the respective unit vector sums  $R_1$ ,  $R_2$  of the two distributions. The classification (A, B, C, or indeterminate) depends on the value of  $\gamma_c$ , with breakpoints at 5, 10 and 20°. The test is negative if  $\gamma > \gamma_c$ . In the Tremp section, the critical angle (at the 95% confidence level) between the two sample mean directions is 9.1°, so the reversal test is positive and classified as B.

The magnetostratigraphy of the Tremp section is characterized by a long reversed polarity zone interrupted by a normal zone. In Fig. 11, the Illerian stratotype is correlated with the geomagnetic polarity time-scale (GPTS) of Berggren et al. (1985). Comparison of the obtained magnetostratigraphy with the paleontological results (Canudo, 1992) shows that the boundary between the Subbotinae and Wilcoxensis biozones is located near the bottom of the normal polarity zone. It coincides with the boundary between

*Morozovella velascoensis* and *Morozovella edgari* (Berggren et al., 1985), between *Globorotalia velascoensis* and *Globorotalia edgari* (Lowrie et al., 1982) and between *Morozovella velascoensis* and *Morozovella subbotinae* s.l. (Cavelier and Pomerol, 1985). According to the Berggren et al. (1985) time-scale, the first normal interval after this boundary corresponds to polarity Chron 24.2. Therefore, the normal polarity interval found in the Illerian stratotype may represent Chron 24.2. The lower and upper reversed intervals of the section are then respectively Chrons 24.1R and 24R. The increase in sedimentation rate towards the top of the section could also explain the absence of Chron 24.1 in the section.

From this correlation, it follows that Chron 24.1R is in the Late Illerian and the upper part of the Middle Illerian, Chron 24.2 is in the middle part of the Middle Illerian and Chron 24R is in the lower part of the Middle Illerian and Early Illerian. If we compare the results obtained in this work with those of an earlier study of shelf facies and magnetostratigraphy (Cavelier and Pomerol, 1985), we may tentatively interpret Chron 25 as belonging to the Paleocene, and Chron 24.1 to the Cuisian (Lower Eocene) (Fig. 11).

#### Acknowledgments

This work was partially supported by a grant from the Science and Education Department of the Spanish Government. Discussions with M.J. Dekkers, R. Molina and A. van Velzen provided helpful and stimulating comments on rock magnetism and magnetostratigraphy. Measurement of the paleontological data was supervised by J.M. Pons and J. Serra-Kiel. C. Puigdefàbregas (Servei Geològic de Catalunya) is thanked for providing the field trip funds. The reversal test program was kindly provided by P.L. McFadden. Funds for paleomagnetic equipment at the Institute of Earth Sciences "Jaume Almera", were provided by the Comisión Internacional de Ciencia y Tecnología (CICYT).

## References

- Aubry, M.P., Berggren, W.A., Kent, D.V., Flynn, J.J., Klitgord, K.D. and Obradovich, J.D., 1988. Paleogene geochronology: an integrated approach. *Paleoceanography*, 3: 707–742.
- Berggren, W.A., Kent, D.V., Flynn, J.J. and van Couvering, J.A., 1985. Cenozoic geochronology. *Geol. Soc. Am. Bull.*, 96: 1407–1418.
- Brookins, D.G., 1988. Eh–pH Diagrams for Geochemistry. Springer-Verlag, Berlin, 176 pp.
- Burbank, D.W. and Puigdefàbregas, C., 1985. Chronologic investigations of the south Pyrenean basins: preliminary magnetostratigraphic results from the Ripoll basin. In: J. Rosell, E. Remacha and M. Zamorano (Editors), 6th European Regional Meeting, 15–17 April, Lerida. Universitat autònoma de Barcelona, pp. 66–69.
- Canudo, J.I., 1992. Los foraminíferos planctónicos del Paleoceno–Eoceno en el Prepirineo meridional y su comparación con la Cordillera Bética. Tesis Doctoral, Univ. Zaragoza, in press.
- Caro, Y., 1973. Contribution à la connaissance des Dinoflagellés du Paléocène–Eocène inférieur des Pyrénées Espagnoles. *Rev. Española Micropaleontol.*, 5: 329–372.
- Casagrande, D.J., 1987. Sulphur in peat and coal. *Geol. Soc. Spec. Publ.*, 32: 87–105.
- Cavelier, C. and Pomerol, Ch., 1986. Stratigraphy of the Paleogene. *Bull. Soc. Géol. Fr.*, 2: 255–265.
- Curry, D., 1981. Thanetien. *Bull. Inf. Géol. Bassin de Paris*, 2: 255–266.
- Dekkers, M.J., 1988. Magnetic behavior of natural goethite during thermal demagnetization. *Geophys. Res. Lett.*, 15 (5): 538–541.
- Dekkers, M.J., 1990. Magnetic monitoring of pyrrhotite alteration during thermal demagnetization. *Geophys. Res. Lett.*, 17: 779–782.
- Ferrer, J., Le Calvez, Y., Luterbacher, H. and Premoli Silva, I., 1973. Contribution à l'étude des foraminifères ilerdiens de la région de Tremp (Catalogne). *Mém. Mus. Natl. Hist. Nat. Paris, Ser. C*, 29, 80 pp.
- Fonnesu, F., 1984. Estratigrafía física y análisis de facies de la Secuencia de Figols entre el río Noguera Pallaresa e Iscles (Prov. de Lérida y Huesca). Tesis Doctoral, Univ. Autònoma de Barcelona, 317 pp.
- Gaemers, P.A.M., 1978. Biostratigraphy and paleogeography of the mainly marine Ager formation (Upper Paleocene–Lower Eocene) in the Tremp Basin, Central–South Pyrenees, Spain. *Leidse Geol. Meded.*, 51: 151–231.
- Hamilton, G.B. and Hojjatzadeh, M., 1982. Cenozoic calcareous nannofossils. A reconnaissance. In: A.R. Lord (Editor), *A Stratigraphical Index of Calcareous Nannofossils*, Vol. 6, Horwood, Chichester, pp. 136–166.
- Heider, F. and Dunlop, D.J., 1987. Two types of chemical magnetization during the oxidation of magnetite. *Phys. Earth Planet. Inter.*, 46: 24–45.
- Hottinger, L. and Schaub, H., 1960. Zur Stufeneinteilung des Paleocaens und des Eocaens. Einführung der Stufen Ilerdien un Biarritzien. Bericht der Schweizerische Palaontologischen Gesellschaft. *Eclogae Geol. Helv.*, 53: 453–479.
- Hottinger, L., 1960. Rechercher sur les alveolines du Paléocène et de l'Eocène. *Mémoires Suisses de Paléontologie*. Basel, 75–76: 245 pp.
- Hottinger, L., Lehmann, R. and Schaub, H., 1964. Données actuelles sur la biostratigraphie du Nummulitique Méditerranéen. *Mém. BRGM*, 28: 611–652.
- Hsieh, K.C. and West, C.A., 1981. Sulfide crystals in coal. *Mater. Sci. Eng.*, 50: 117–125.
- Kapellos, C. and Schaub, H., 1973. Zur Korrelation von Biozönierungen mit Grossforaminiferen und Nannoplankton im Paläogen der Pyrenaen. *Eclogae Geol. Helv.*, 66: 687–737.
- Kapellos, C. and Schaub, H., 1975. L'Ilerdien dans les Alpes, dans les Pyrénées et en Crimée. Correlation de zones grands Foraminifères et Nannoplankton. *Bull. Soc. Géol. Fr.*, 17: 148–161.
- Kirschvink, J.L., 1980. The least-squares line and plane and the analysis of palaeomagnetic data. *Geophys. J.R. Astron. Soc.*, 62: 699–718.
- Kligfield, R. and Channell, J.E.T., 1981. Widespread remagnetization of Helvetic limestones. *J. Geophys. Res.*, 86 (B3): 1888–1900.
- Krs, M., Novák, F. et al., 1992. Magnetic properties and metastability of greigite-smythite mineralisation in brown-coal basins of the Krušné hory Piedmont, Bohemia.
- Linssen, J.H., 1988. Preliminary results of a study of four successive sedimentary geomagnetic reversal records from the Mediterranean (Upper Thvera, Lower and Upper Sidufjall, and Lower Nunivak). *Phys. Earth Planet. Inter.*, 52: 207–231.
- Lowrie, W., 1990. Identification of ferromagnetic minerals in a rock by coercivity and unblocking temperature properties. *Geophys. Res. Lett.*, 17 (2): 159–162.
- Lowrie, W., Alvarez, W., Napoleone, G., Perch-Nielsen, K., Premoli Silva, I. and Toumarkine, M., 1982. Paleogene magnetic stratigraphy in Umbrian pelagic carbonate rocks: The Contesa sections, Gubbio. *Geol. Soc. Am. Bull.*, 93: 414–432.
- Luterbacher, H., 1973. La sección tipo del Ilerdiense. In: C.N.G. Enadinsa (Editor), XIII Coloquio Europeo de Micropaleontología, September 18–27, Madrid, pp. 113–140.
- Martini, E., 1971. Standard Tertiary and Quaternary calcareous nannoplankton zonation. In: *TECNOSCIENZA* (Editor), Proc. 2nd Int. Conf. Plankt. Microfossils, Roma, Vol. 20, pp. 739–785.
- McFadden, P.L. and McElhinny, M.W., 1990. Classification of the reversal test in palaeomagnetism. *Geophys. J. Int.*, 103: 725–729.
- Mey, P.H.W., Nagtegaal, P.J.C., Roberti, K.J. and Hattevelt, J.J.A., 1968. Lithostratigraphic subdivision of post-Hercynian deposits in the South–Central Pyrenees, Spain. *Leidse Geol. Meded.*, 41: 221–228.
- Molina, E., Canudo, J.I., Guernet, C., McDougall, K., Ortiz, N., Pascual, J.O., Parés, J.M., Samso, J.M., Serra-Kiel, J. and Tosquella, J., 1992. The stratotypic Ilerdian revisited:

- Integrated Stratigraphy across the Paleocene/Eocene boundary. *Rév. Micropaléontol.*, 35 (2): 143–156.
- Morse, J.W., Millero, F.J., Cornwell, J.C. and Rickard, D., 1987. The chemistry of hydrogen sulfide and iron sulfide systems in natural waters. *Earth-Sci. Rev.*, 24: 1–42.
- Mutti, E., Séguret, M. and Sgaretti, M., 1988. Sedimentation and Deformation in the Tertiary Sequences of the Southern Pyrenees. AAPG Mediterranean Basins Conf., 25–28 September, Nice. Institute of Geology, University of Palma, Palma, Field Trip 7: 157 pp.
- Mutti, E., Luterbacher, H.P., Ferrer, J. and Rosell, J., 1972. Schema stratigrafico e lineamenti di facies del Paleogene marino della zona centrale sudpirenaica tra Tremp (Catalogna) e Pamplona (Navarra). *Mem. Soc. Geol. Ital.*, 11: 319–416.
- Özdemir, Ö., 1990. High-temperature hysteresis and thermoremanence of single-domain maghemite. *Phys. Earth Planet. Inter.*, 65: 125–136.
- Parés, J.M., 1988. Dades paleomagnètiques del NE de la placa Ibèrica: implicacions tectòniques. Tesis Doctoral, Univ. Barcelona, 378 pp.
- Parés, J.M., Banda, E. and Santanach, P., 1988. Paleomagnetic results from the southeastern margin of the Ebro Basin (northeastern Spain): evidence for a Tertiary clockwise rotation. *Phys. Earth Planet. Inter.*, 52: 267–282.
- Pascual, J.O. and Parés, J.M., 1990. Estudio preliminar de los materiales comprendidos en el tránsito Eoceno–Oligoceno en el borde SE de la Cuenca del Ebro. *Rev. Soc. Geol. Esp.*, 3: 323–333.
- Pascual, J.O., Samsó, J.M., Tosquella, J., Parés, J.M. and Serra-Kiel, J., 1991. Magnetostratigrafia y biostratigrafía del estratotipo del Illerdiense (Tremp, Lleida). In: F. Colombo, E. Ramos-Guerrero and S. Sierra (Editors), I Congreso del grupo Español del Terciario, Vic. 18–20 March. Abstract, pp. 224–247.
- Perch-Nielsen, K. and Hasen, J.M., 1981. Selandian. *Bull. Inf. Géol. Bassin de Paris*, 2: 219–230.
- Puigdefàbregas, C. and Souquet, P., 1986. Tectono-sedimentary cycles and depositional sequences of the Mesozoic and Tertiary from the Pyrenees. *Tectonophysics*, 129: 173–203.
- Schaub, H., 1969. L'Illerdien, état actuel du problème. *Mém. BRGM*, 69: 259–266.
- Schaub, H., 1981. Nummulites et Assilines de la Téthys Paléogène. Taxonomie, phylogénèse et biostratigraphie. *Mém. Suiss. Paléontol.*, 104–106: 236 pp.
- Souquet, P., Peybernes, B., Bilotte, M. and Debboas, E.J., 1977. La chaîne alpine des Pyrénées. *Geol. Alp.* e, 53: 193–216.
- Steurbaut, E., 1988. New Early and Middle Eocene calcareous-nannoplankton events and correlations in middle to high latitudes of the northern hemisphere. *News. Stratigr.*, 18: 99–115.
- Van der Voo, R., 1990. Phanerozoic paleomagnetic poles from Europe and North America and comparisons with continental reconstructions. *Rev. Geophys.*, 28: 167–206.
- Van Velzen, A.J. and Zijdeveld, J.D.A. 1992. A method to study alterations of magnetic minerals during thermal demagnetization applied to a fine-grained marl (Trubi Formation, Sicily). *Geophys. J. Int.*, 110: 79–90.
- von Hillebrandt, A., 1975. Correlations entre les biozones de grands Foraminifères et des Foraminifères planctoniques de L'Illerdien. *Bull. Soc. Géol. Fr.*, 7: 162–167.
- Wilcoxon, J.A., 1973. Paleogene calcareous nannoplankton from the Campo and Tremp sections of the Illerian stage in NE Spain. *Rev. Esp. Micropaleontol.*, 5: 107–112.
- Williams, G.D., 1985. Thrust tectonics in the south central Pyrenees. *J. Struct. Geol.*, 7: 11–17.